Simulated Photo-nuclear Kaon Production Analysis for LDMX

Chloe Greenstein, Lewis & Clark College

Advisor: Cristina Mantilla Suárez , Fermilab National Accelerator Laboratory

Abstract

In this study, we explore the production of Kaons in rare photonuclear (PN) processes in the Light Dark Matter Experiment (LDMX). LDMX uses electron fixed-target reactions to search for light dark matter in the sub-GeV region. Photonuclear processes, where a hard Bremsstrahlung photon undergoes a photo-nuclear reaction in the target, are a challenging background for LDMX. These processes can produce single particles, such as Kaons, that carry most of the photon's energy and later decay into semi-visible signatures. In this study, we explore the event rates and kinematics of PN neutral Kaons with fully visible decays. We estimate the capability of LDMX to reconstruct these decays and use them to estimate the rate of semi-visible PN decays, such as those originating from K-long decays.

Introduction

The Light Dark Matter Experiment, LDMX, is a proposed accelerator experiment for detecting sub-GeV dark matter. LDMX looks for dark matter produced in feebly mediated interactions between dark matter and Standard Model Particles. The search range covers dark matter masses between 1 MeV and 1 GeV. This mass regime is experimentally accessible and is further motivated by the hypothesis that reactions of dark matter in the early universe gave rise to the appropriate abundance of dark matter post-annihilation. Therefore, LDMX will probe light dark matter models where a minimum interaction strength between dark and ordinary matter is expected.

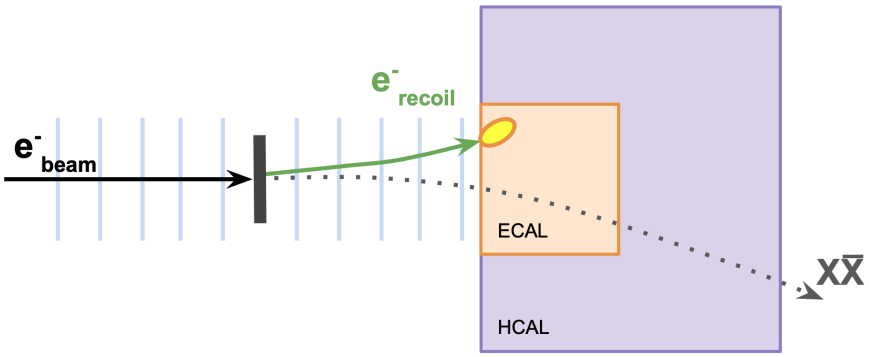

Fig. 1.— Conceptual drawing of the LDMX experiment, showing the electron beam passing through a tagging tracker, impacting on a fixed-target, the recoil tracker, the electromagnetic calorimeter, and hadron calorimeter.

The experiment aims a 4 GeV electron beam at a fixed-target. The beam travels through a tagging tracker before hitting the 50-micron wide tungsten target. Particles then travel through the

recoil tracker, an electromagnetic calorimeter (ECAL), and a hadronic calorimeter (HCAL). An schematic of the experiment is shown in Figure 1. The combination of these detectors can account for all Standard Model particles and the electron initial energy. Dark matter can then be responsible for the lost energy. The process for vetoing backgrounds thus requires a deep understanding of the various Standard Model energy carriers.

Photo-nuclear (PN) processes, where a hard Bremsstrahlung photon undergoes a photo-nuclear reaction in the target or in the ECAL, provide a challenging background to measure. These processes can produce single particles that carry most of the photon's energy and later decay into semi-visible signatures. The rate of this background occurring in the target is 1.5e-3 per incident electron (Åkesson et al. (2020)).

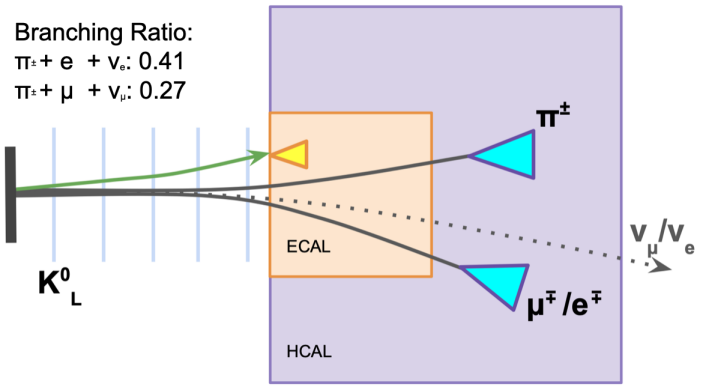

Fig. 2.— Conceptual drawing of the LDMX experiment, showing the path of the products of K_L decay from a fixed-target, through the recoil tracker, the electromagnetic calorimeter, and hadron calorimeter.

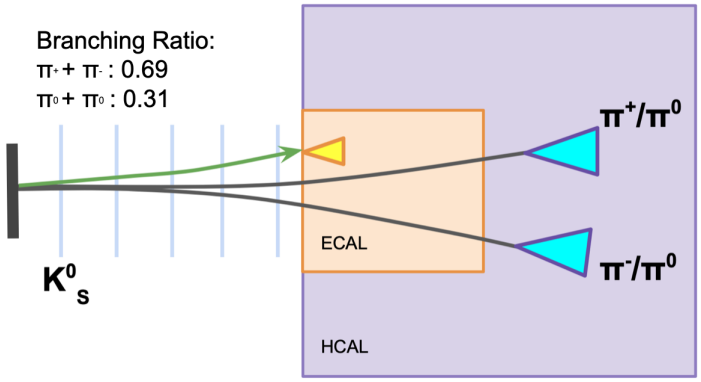

Fig. 3.— Conceptual drawing of the LDMX experiment, showing the path of the products of K_S decay from a fixed-target, through the recoil tracker, the electromagnetic calorimeter, and hadron calorimeter.

This study examines the LDMX detector's ability to reconstruct photo-nuclear (PN) backgrounds in a data-driven way, by measuring visible decays of a neutral Kaon. K-short (K_S) decays into charged pions, with a branching ratio of 0.692 (Particle Data Group et al. (2020)), can be fully reconstructed in the ECAL as two separate showers. K-long (K_L) decays, in the other hand, will produce neutrinos. Schematics of both decays are shown in Figures 2,3. In this study we obtain

the yields and kinematics of K_S decays in the detector simulation and translate them into expected rates of the K_L background.

Simulation Methods

This study uses simulated PN interactions to evaluate neutral kaon production. 4 GeV PN events are computationally generated using a GEANT4-based model. These events require a Bremsstrahlung process in the target region with photon energy greater than 2.5 GeV. This parameter implies recoil electron energy is less than 1.5 GeV. An schematic of this process is shown in Fig. 4.

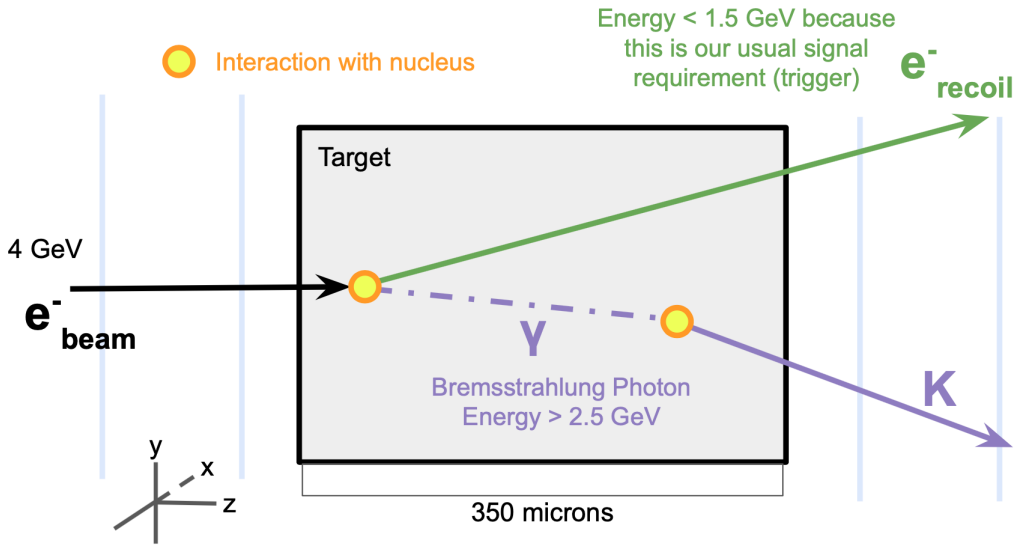

Fig. 4.— Conceptual drawing of the generated PN event, showing the electron beam passing through a tagging tracker, impacting on a fixed-target, producing a Bremsstrahlung photon. The photon impacts on a nuclear producing a Kaon. The simulation parameters are labeled as such.

Since the production cross section of this process is so small, an arbitrary large bias factor on the scale of 1e9 is applied to the cross-section. This bias factor allows fewer events to be run and a larger sample of Kaon events. The biased generation produces K_S at a rate of one truth K_S per 48 events generated. For comparison, non-biased generation produces about 1 truth K_S per 50,000 events. With 1e16 EOT (electrons on target), the expected luminosity of LDMX, 1.7e-5 PN background events are expected producing 3.4e6 K_S. The simulation saves all decay products of the kaons at the generator level; no assumptions are made about detector effects. As visible in Figure 5, the K_L and K_S production rate in these events is similar.

Truth K_S and K_L kinetic energies are shown against the recoil electron's energy in Figure 6. We observe a large number of lower energy Kaons. The first upper limit on the diagonal axis is due to cases where the Kaon is produced in association with other Kaons. We also observe a higher band due to PN events where only one Kaon is produced in the events. Most importantly, the distribution of events are very similar between K_L and K_S. Their matching distribution motivates the use of K_S to account for K_L.

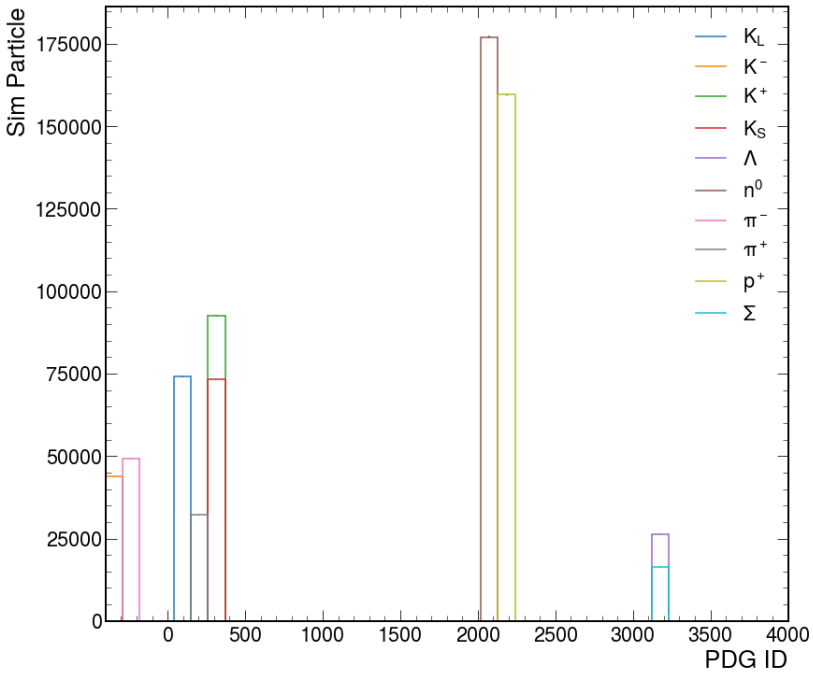

Fig. 5.— Histogram representing the PDG ID of particles generated in the PN generator. This plot includes particles with the top two highest kinetic energies per event.

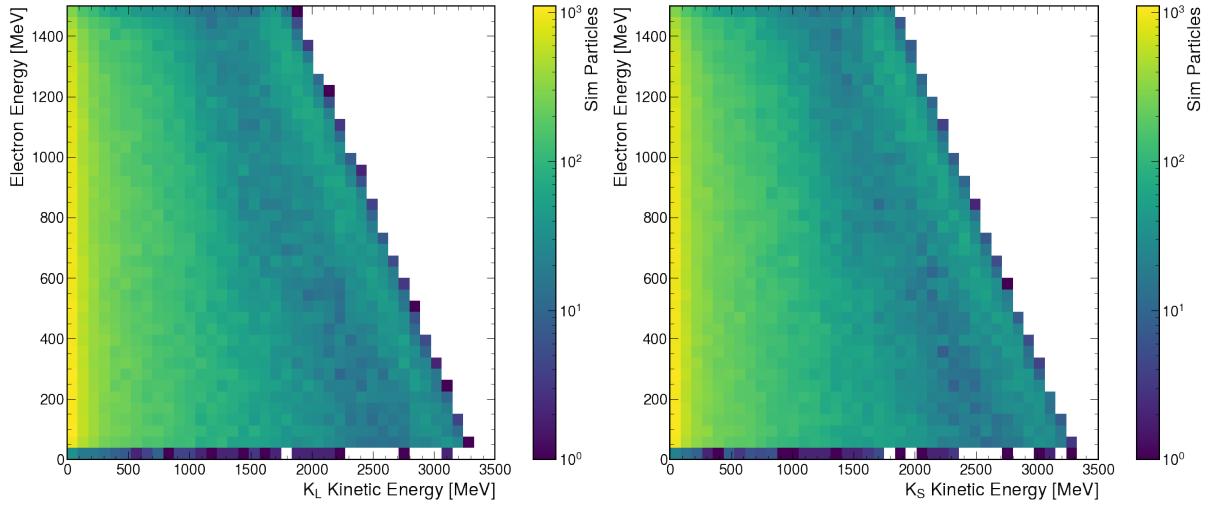

Fig. 6.— 2D Histogram representing the kinetic energy of Kaons vs recoil electron energy. From left to right, these plots account for truth K_L and truth K_S.

Truth Kaon Ratios

The reconstruction of K_L from K_S assumes the ratio of production to be one to one. To determine the validity of this assumption, the ratio of K_L to K_S is examined for multiple scenarios. The ratio for all truth Kaons is shown in Figure 7. The plot hovers around a 1:1 match until the highest

kinetic energy grouping, where there are far fewer truth Kaons in the dataset.

Only the particles with the highest or second-highest kinetic energy in each event are then saved. These events are split up depending on particles produced with the Kaons of interest. The ratio of events where a single Kaon is produced is displayed in Figure 8. The data selection for this case is large, and the ratios closely resemble the distribution of Figure 7. Events with another Kaon produced in association with the neutral Kaon are examined in Figure 9. Finally, events where Kaons are produced with other high energy particles, Lambda and Sigma, are shown in Figure 10 and Figure 11.

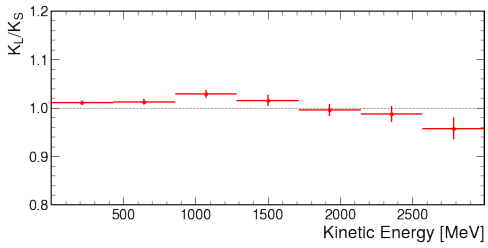

Fig. 7.— Ratio of all truth K_L and K_S from PN generator divided across kinetic energy distribution.

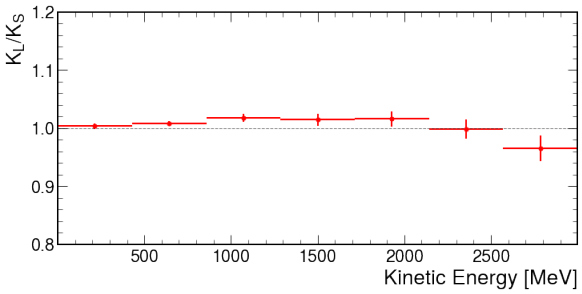

Fig. 8.— Ratio of selected truth K-long and K-short from PN generator divided across kinetic energy distribution. Includes particles of highest kinetic energy per event. Kaons selected from cases a single Kaon is produced.

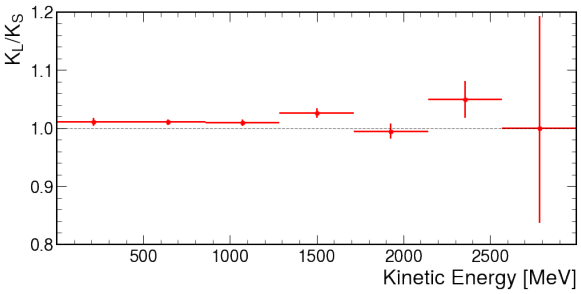

Fig. 9.— Ratio of selected truth K-long and K-short from PN generator divided across kinetic energy distribution. Includes particles of highest kinetic energy per event. Kaons selected from cases where a second Kaon is produced.

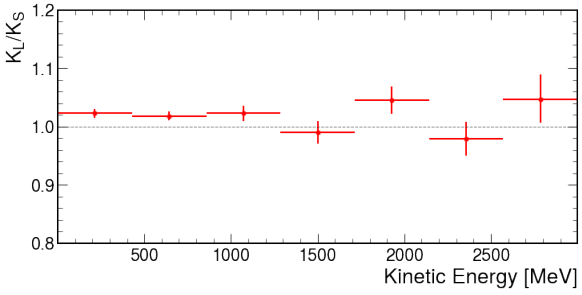

Fig. 10.— Ratio of selected truth K-long and K-short from PN generator divided across kinetic energy distribution. Includes particles of highest kinetic energy per event. Kaons selected from cases a single Kaon and a single Lambda are produced.

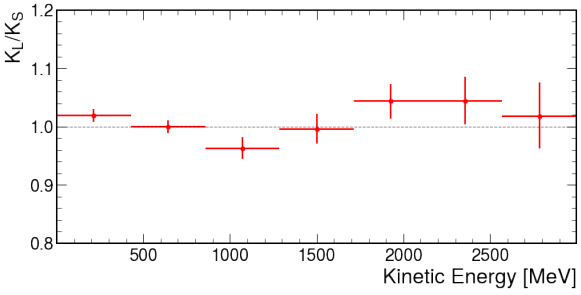

Fig. 11.— Ratio of selected truth K-long and K-short from PN generator divided across kinetic energy distribution. Includes particles of highest kinetic energy per event. Kaons selected from cases a single Kaon and a single Sigma are produced.

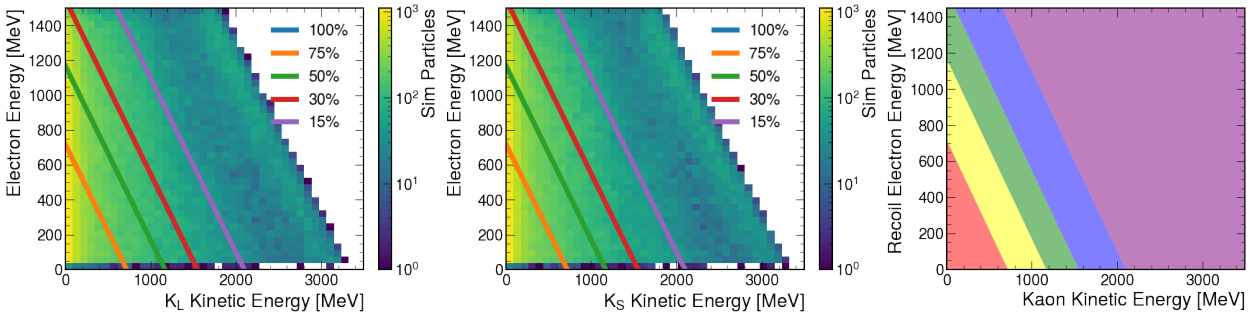

Fig. 12.— Kinetic energy distributions of the K-long (left) and K-short (middle) as a function of the electron's recoil energy in PN events. The 2D distribution is split in bands that show different kinetic regions of interest.

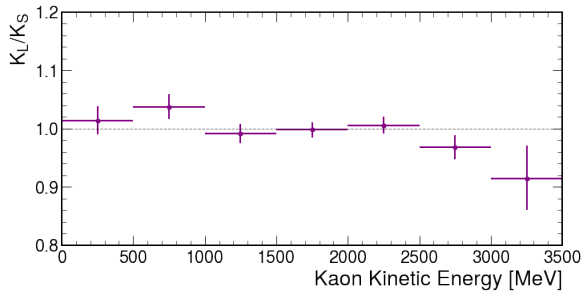

Fig. 13.— Ratio of truth K-long to K-short in the purple percentile, the top 15%.

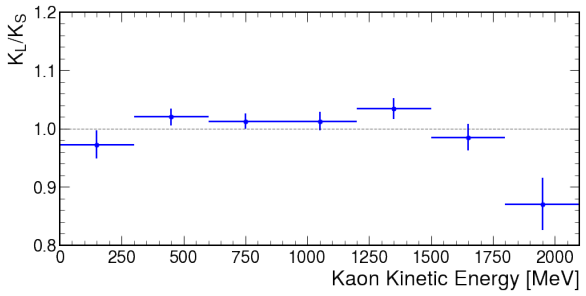

Fig. 14.— Ratio of truth K-long to K-short in the blue percentile, the top 15-30%.

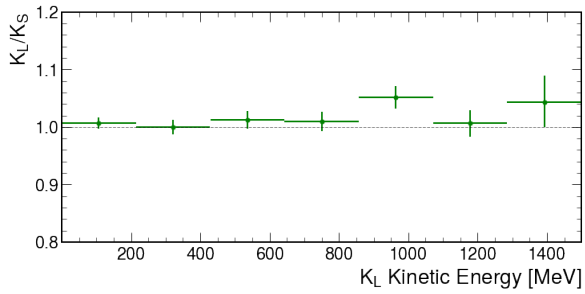

Fig. 15.— Ratio of truth K-long to K-short in the green percentile, the top 30-50%.

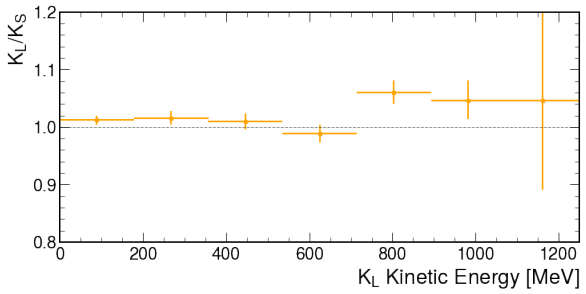

Fig. 16.— Ratio of truth K-long to K-short in the yellow percentile, the top 50-75%.

The data is divided into bands representing the percentile of kinetic energy versus recoil electron energy to compare the rate of truth K_L and K_S at different kinematics. In the largest percentile, the Kaons have taken the most energy and provide the ideal sample for comparison with K_L. The ratio of truth K_L to K_S is then taken for each of the five percentile ranges.

These ratios show that in multiple types of events and different energy levels, the ratio of truth K_L to K_S remains around one. This relation suggests K_S can be used to account for the semi-visible decays of K_L.

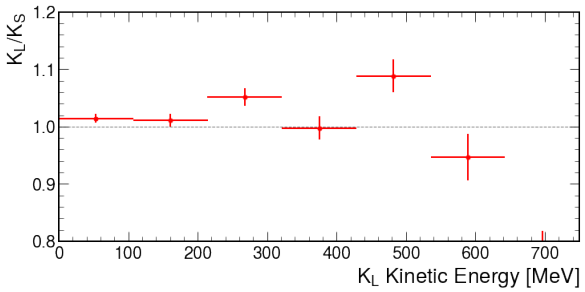

Fig. 17.— Ratio of truth K-long to K-short in the red percentile, the top 75-100%.

Reconstructing K-Short

From Figure 2, K_S decays into charged pions are observable in both the ECAL and HCAL. To reconstruct these Kaons, we assume the momentum of their decay products in the x, y, and z directions and energy are known. Using the Lorentz vectors of the pions, the energy of pions in the same event are then summed. The resulting energy plot (Figure 19) has a resonance around 498 MeV, the mass of K_S.

Detector observables, momentum in the x, y, and z dimensions, are simulated while processing the data. The simulation truth values perfectly reconstruct kaon masses from daughters. Smearing is applied to the three variables to account for detector uncertainties estimated by Åkesson et al. (2020). This paper outlines uncertainty of momentum as dependent on its magnitude. The piecewise equations used are as follows:

Px [MeV]	Uncertainty
0<px<100	3.00 MeV
100<px<500	3.20 MeV
500<px<1000	3.40 MeV
1000<px<1300	3.50 MeV
1300<px	3.85 MeV

Py [MeV]	Uncertainty
0<py<100	3.75 MeV
100<py<350	3.80 MeV
350<py<500	4.20 MeV
500<py<1000	4.80 MeV
1000<py<1200	4.98 MeV
1200<py<2000	3.85 MeV
200<py	5.50 MeV

Pz [MeV]	Uncertainty
0<pz<50	4.04%
50<pz<100	4.10%
100<pz<250	4.15%
250<pz<500	4.20%
500<pz<1000	4.35%
1000<pz<2000	4.77%
2000<pz<3000	5.23%
3000<pz<4000	5.73%
4000<pz	6.00%

Fig. 18.— The piecewise functions defining momentum uncertainty along the x axis (left), y axis (middle), and z axis (right). The uncertainty is dependent on the magnitude of the momentum in either percentage or MeV.

This smearing is applied for all decay daughters. Additionally, daughters of these interactions that do not reach detectors must be taken into account. In order to account for LDMX's angle acceptance, we only include particles with a θ angle less than 40° from the z-axis (along the beam

line). This requirement is applied to all the decay daughters. The mass resolution that we estimate is in the order of 20 GeV.

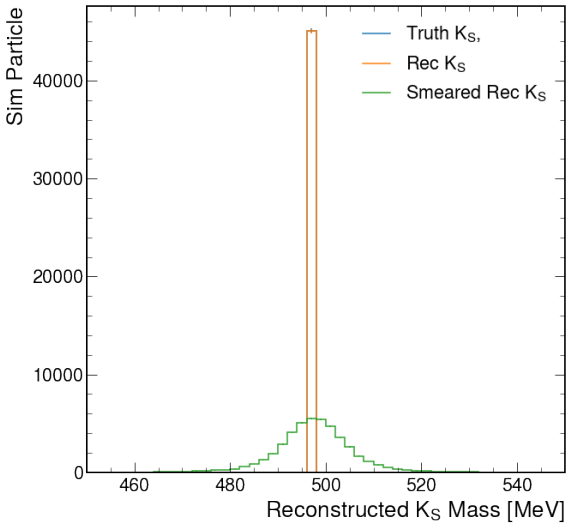

Fig. 19.— Reconstructed K_S mass from its charged pion decays accounting for detector effects (green) and truth Kaon mass (orange and blue).

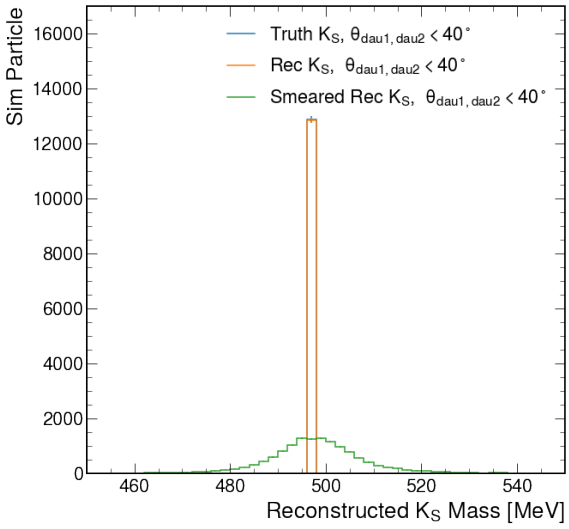

Fig. 20.— Reconstructed K_S mass from its charged pion decays accounting for detector effects (green) and truth Kaon mass (orange and blue) within the LDMX detector acceptance.

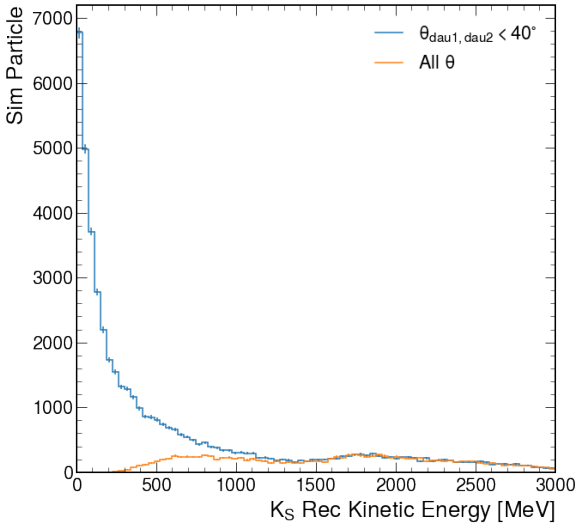

bht

Fig. 21.— Distribution of the K_S kinetic energy for all reconstructed Kaons and those within angle acceptance.

Finally, we plot the kinetic energy of these reconstructed K_S and see a direct correlation of high energy Kaons and daughters within angle acceptance.

Like the truth kaons, the data is divided into kinematic regions by percentiles. Using the percentiles, the ratio is found in each kinematic region as shown in Figure 12. The ratio of all

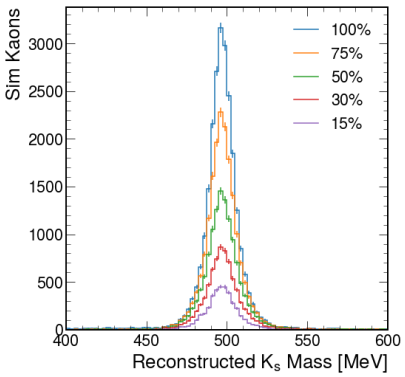

Fig. 22.— Mass resolution for K_S reconstructed from charged Kaon decays for different percentiles of the PN energy distribution (See text).

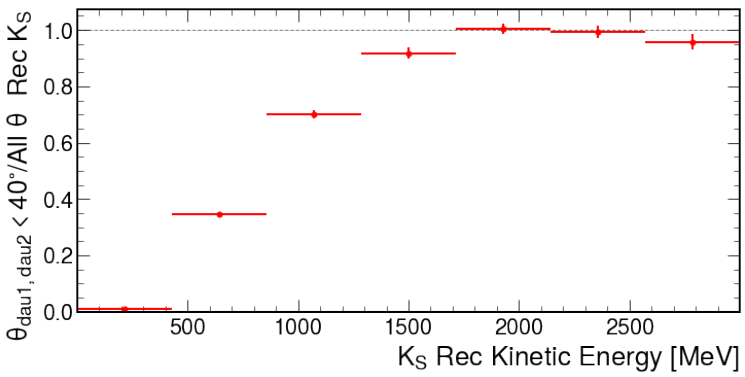

Fig. 23.— Ratio of events with a K_S within detector acceptance with respect to all K_S.

reconstructed kaons to reconstructed kaons with daughters under the theta acceptance represents the overall acceptance for detecting these kaons through reconstruction.

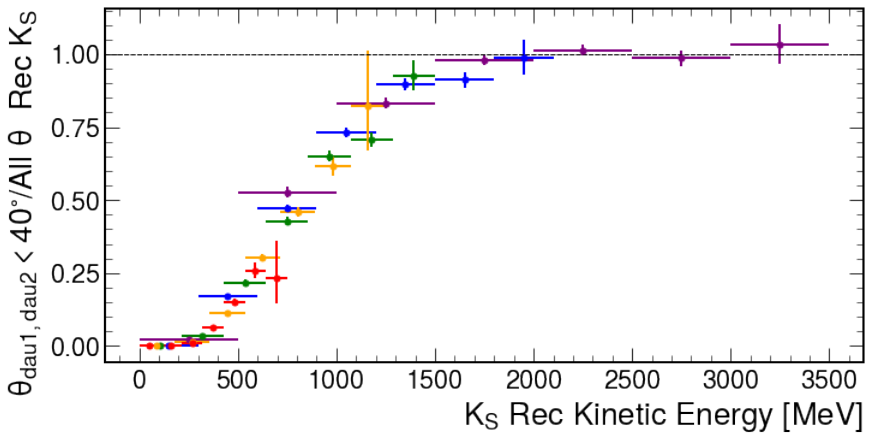

Fig. 24.— Ratio between K_S that are within the angle acceptance of LDMX ($\theta < 40$ deg) and the total number of K_S generated in our sample.

The energy range matters more with the theta acceptance. There are very few Kaons with daughters that pass the angle requirement with low energy. There is a cut-off around 300 MeV in kinetic energy where the daughters have kinematics at angles out of acceptance. However, the higher kinematic regions are unaffected by the angle requirement. The θ acceptance requirement removes few K_S with higher energy. Taking smearing and the angle acceptance into account, these acceptances must be considered in calculating K_L.

Reconstructing K-Long from K-Short

Given the simulated conditions and detector sensitivity uncertainty, the neutrino background from K_L decay can be determined using K_S decay analysis. These K_L can be described by using the following equations.

The branching ratio of K_S into pions is defined as:

$$K_s = \frac{K_s(\pi^+\pi^-)}{BR_{\pi^+\pi^-}}, \tag{1}$$

and measured constant, 0.692 (Particle Data Group et al. (2020)).

The ratio of K_S to K_L measured is applied to solve for

$$K_L = \frac{K_L}{K_s} * \frac{K_s(\pi^+\pi^- : measured)}{BR_{\pi^+\pi^-}}, \tag{2}$$

where the fraction of K_S that can be measured takes into account the angle acceptance through the equation:

$$K_s(\pi^+\pi^- : measured) = K_s(\pi^+\pi^- : truth) * Acceptance(\theta_{\pi^+\pi^-} < 40^\circ). \tag{3}$$

This equation can then be plugged into (3).

$$K_L = \frac{K_L}{K_s} * K_s(\pi^+\pi^- : truth) * \frac{Acceptance(\theta_{\pi^+\pi^-})}{BR_{\pi^+\pi^-}} \tag{4}$$

These equations show how the studies above can account for rates of K_L produced in PN interactions.

Conclusion

These studies determine that visible PN decays of K_S can be successfully reconstructed in order to estimate the semi-visible PN decays of K_L. Production of K_S and K_L are related with a ratio of about 1:1 in all kinematic regions and events. In the many kinematic regions studied, the truth K_S and K_L distributions are identical. K_S can be successfully reconstructed using visible pion daughters, with a mass resolution of $\sim$ 20 GeV.

These methods can be further tested for other necessary veto handles in LDMX. Reconstruction of heavier particles, Lambda and Phi, were also attempted. Lambda was successfully reconstructed using daughters n^0, and π^0 with a branching ratio of 0.358 Olive et al. (2014). With the smearing and theta acceptance, the mass was reconstructed with an uncertainty of 6 MeV.

This research will next look into K^+ (K-plus) production. K^+ will produce a neutrino background through its decay into μ, and ν_μ with a branching ratio of 0.64 Tanabashi et al. (2018). Unlike neutral Kaons, K^+ could differ from K_S and K_L rates by a factor of about three Compton et al. (2017). The difference is more significant at higher energies. K^+ can be reconstructed (like the K_S) from daughters π^+, π^+, and π^- with a branching ratio of 0.06. This smaller branching ratio and longer lifetime indicate that only a small sample of these daughter pions can be detected. This reconstruction may require alternative approaches such as the measurement of energy lost or the measurement of the Kaon time of flight.

Thank you to the LDMX team at Fermilab National Accelerator Laboratory for the research opportunity. Thank you especially to this project's supervisor, Cristina Mantilla Suárez, for her

expertise and guidance. Thank you, Nhan Tran and Christian Herwig, for your advice and encouragement in the LDMX project. I would also like to thank the SIST leadership at Fermilab for their mentorship and investment in educating future researchers.

References

Åkesson, Torsten, Blinov, Nikita, Bryngemark, Lene, Colegrove, Owen, Collura, Giulia, Dukes, Craig, . . . Whitbeck, Andrew. (2020). A high efficiency photon veto for the Light Dark Matter eXperiment. The Journal of High Energy Physics, 2020(4), 1-35.

Åkesson, Torsten, Berlin, Asher, Blinov, Nikita, Colegrove, Owen, Collura, Giulia, Dutta, Valentina, . . . Whitbeck, Andrew. (2018).

Ankowski, Artur M, Friedland, Alexander, Li, Shirley Weishi, Moreno, Omar, Schuster, Philip, Toro, Natalia, & Tran, Nhan. (2020). Lepton-nucleus cross section measurements for DUNE with the LDMX detector. Physical Review. D, 101(5), Physical review. D, 2020-03, Vol.101 (5).

Compton, N, Hicks, K, Cole, P, Zachariou, N, Ilieva, Y, Klempt, E, . . . Zhang, J. (2017). Measurement of the differential and total cross sections of the γd$\rightarrow$K0λ(p) reaction within the resonance region. Physical Review. C, 96(6), Physical review. C, 2017-12, Vol.96 (6).

L. Garren F. Krauss C.-J. Lin S. Navas P. Richardson T. SjSstrand. "MONTE CARLO PARTICLE NUMBERING SCHEME." Chinese Physics C, no. 10, 2016, pp. 553–556.

Olive, K. A, Agashe, K, Amsler, C, Barnett, R. M, Bichsel, H, Biebel, O, . . . Harper, G. (2014). REVIEW OF PARTICLE PHYSICS Particle Data Group. Chinese Physics C, High Energy Physics & Nuclear Physics, 38(9), Chinese Physics C, High Energy Physics & Nuclear Physics, 2014, Vol.38 (9).

Particle Data Group, Groom, D. E, Antonelli, M, Aschenauer, E. C, Baer, H, Baudis, L, . . . Zimmermann, F. (2020). Review of Particle Physics. Progress of Theoretical and Experimental Physics, 2020(8), Progress of theoretical and experimental physics, 2020-08-07, Vol.2020 (8).

Tanabashi, M, Hagiwara, K, Hikasa, K, Nakamura, K, Sumino, Y, Takahashi, F, . . . Hernández-Rey, JJ. (2018). Review of Particle Physics. Physical Review. D, 98(3), Physical review. D, 2018-08-01, Vol.98 (3).